CONVOLUTION KERNEL COMPENSATION APPLIED TO 1D AND 2D BLIND SOURCE SEPARATION

Damjan Zazula, Aleš Holobar, Matjaž Divjak

Faculty of Electrical Engineering and Computer Science, University of Maribor
Smetanova 17, 2000 Maribor, Slovenia

Abstract: Many practical situations can be modelled with multiple-input multiple-output (MIMO) models. If the input sources are mutually orthogonal, several blind source separation methods can be used to reconstruct the sources and model transfer channels. In this paper, we derive a new approach of this kind, which is based on the compensation of the model convolution kernel. It detects the triggering instants of individual sources, and tolerates their non-orthogonalities and high amount of additive noise, which qualifies the method in several signal and image analysis applications where other approaches fail.. We explain how to implement the convolution kernel compensation (CKC) method both in 1D and 2D cases. This unified approach made us able to demonstrate its performance in two experiments. A 1D application was introduced to the decomposition of surface electromyograms (SEMG). Nine healthy males participated in the tests with 5% and 10% maximum voluntary isometric contractions (MVC) of biceps brachii muscle. We identified 3.4 ± 1.3 (mean $\pm$ standard deviation) and 6.2 ± 2.2 motor units (MUs) at 5% and 10% MVC, respectively. At the same time, we applied the 2D version of CKC to range imaging. Dealing with the Middlebury Stereo Vision referential set of images, our method found correct matches of $91.3 \pm 12.1\%$ of all pixels, while the obtained RMS disparity difference was 3.4 ± 2.5 pixels. This results are comparable to other ranging approaches, but our solution exhibits better robustness and reliability.

1 INTRODUCTION

Blind source separation (BSS) has matured to a very well established theory which has given a fresh impetus to several applications in different research fields. If a problem can be modelled in multiple-input multiple-output sense (MIMO) and the input excitations of such a model can be considered orthogonal sources, many BSS techniques are available to separate those sources. Robust and useful solutions have been reported for telecommunications (Madhow, 1998), seismic and radar signals (Desodt, 1994), speech processing (Gribonval, 2002), bioelectric signals (Barros, 1999), image processing (Hyvärinen, 2002), etc.

The majority of BSS-based approaches take advantage of the sources' orthogonality. Several observations, i.e. the output signals of the presumed MIMO model, are taken into account referring to their mutual information contents, such as covariance.

The covariance-based techniques build a covariance matrix which comprises the information on the model transfer channels, i.e. the model convolution kernel, and the covariance of sources. Actually, the source covariance matrix appears to be diagonal, which unveils the convolution kernel. The information on the convolution kernel is, afterwards, used to deconvolve also the original source signals (Cardoso, 1998), (Belouchrani, 1997).

However, there are two major drawbacks that degrade the success of BSS in certain cases, which is when the number of observations is lower than the number of sources and when the sources lack the orthogonality. The both drawbacks prevent a proper identification of the convolution kernel, which hinders applications in the biomedical field, for example. The obtained shapes of source signals and modelled channel responses are distorted because they are projected into an orthogonal space, in underdetermined cases also with lower number of dimensions as

needed. So, the obtained results equal unknown linear combinations of the original sources and channel responses.

Recently, a novel approach was proposed which successfully separates the contributions of sources even if they are only close-to-orthogonal and if the number of observations is underdetermined (Holobar, 2004). It is based on the fact that there is variety of situations where sources produce only a limited number of finite symbols (source activity). Being sent through the transfer channel, those symbols are convolved with the channel responses and they appear in the observations as the contributions of symbols. If, for example, bioelectric signals are considered, electrocardiograms (ECG) can be modelled with fully orthogonal sources (there is no overlap possible between different types of heart beats, such as normal systoles and extrasystoles), while electromyograms (EMG) lose orthogonality with increasing contraction forces (motor-unit action potentials exhibit more overlapping) (De Luca, 1996). On the other hand, observing certain types of communications, such as CDMA (Madhow, 1998), orthogonality of sources may be supposed as well. Moreover, we are not constrained to 1D; similar reasoning may be extended to 2D images. If an image is taken as a MIMO output observation, it can also be considered the result of some source activities transferred through the model channels. In this case, sources produce symbols in the form of 2D regions (subimages that contribute to the observed image), and are expected to be orthogonal (subimages do not overlap).

Given a number of observations of some sources, the contributions produced by the transferred source symbols may be characterized by their shape and appearance (triggering) instants. Stationarity is also supposed both for the sources and for the model channels. We have developed a method which makes use of the abovementioned facts and detects the triggering instants of the same symbols as they appear in the observation. Our method actually compensates the detected shape of the observed source contributions. The approach turned out to be Bayesian optimal (Kay, 1993).

The paper continues as follows: Section 2 reveals the novel method called convolution kernel compensation (CKC) and extends it from 1D to 2D, Section 3 explains its application to surface EMG signals, while section 4 shows the method's efficiency when applied to range imaging in stereo vision. The paper is concluded by Section 5.

2 DETECTION OF SOURCE-SYMBOL TRIGGERING INSTANTS

Consider the following data model:

$$y_i(n) = \sum_{j=1}^{K} \sum_{l=0}^{L-1} c_{ij}(l) t_j(n-l) + v_i(n); i = 1, \ldots, M \quad (1)$$

where $y_i(n)$ stands for the i-th observation, $c_{ij}(l)$ corresponds to the contribution of length L of the j-th source symbol in the i-th observation, and $t_j(n-l)$ denotes a sequence of triggering instants for this symbol, $t_j(n) = \sum_{l=-\infty}^{\infty} \delta(n - T_j(l))$, with unit-sample pulses placed at $T_j(l)$ lags, while $v_i(n)$ is considered i.i.d. white noise independent from the sources.

It has been shown 0 that Eq. (1) can be transformed into a multiplicative vector form as follows:

$$\mathbf{y}_e(n) = \mathbf{C}_e \mathbf{t}_e(n) + \mathbf{v}_e(n); n = 0, \ldots, N-1 \quad (2)$$

where subscript e designates extended vectors and matrices, $\mathbf{C}_e$ contains the observed contributions of source symbols,:

$$\mathbf{C}_e = \begin{bmatrix} \mathbf{C}_{11} & \cdots & \mathbf{C}_{1K} \\ \vdots & \ddots & \vdots \\ \mathbf{C}_{M1} & \cdots & \mathbf{C}_{MK} \end{bmatrix} \quad (3)$$

with

$$\mathbf{C}_{ij} = \begin{bmatrix} c_{ij}(0) & \cdots & c_{ij}(L-1) & \cdots & 0 \\ \vdots & \ddots & \ddots & \ddots & \vdots \\ 0 & \cdots & c_{ij}(0) & \cdots & c_{ij}(L-1) \end{bmatrix}, \quad (4)$$

$\mathbf{y}_e(n)$ stands for the extended vector of observations, and $\mathbf{t}_e(n)$ for the vector of triggering pulses, both at lag n:

$$\mathbf{y}_e(n) = [y_1(n), \ldots, y_1(n-M_e+1), \ldots, y_M(n), \ldots,$$
$$y_M(n-M_e+1)]^T$$
$$\mathbf{t}_e(n) = [t_1(n), \ldots, t_1(n-L-M_e+2), \ldots, t_K(n), \ldots,$$
$$t_K(n-L-M_e+2)]^T$$
$$(5)$$

Extended noise vector $\mathbf{v}_e(n)$ is considered constructed in the same way.

M_e from Eqs. (5) means an extension factor. If it fulfils the following inequality

$$M \cdot M_e \geq K(L + M_e - 1), \quad (6)$$

then for K different observed symbols of length L and M observations the matrix $\mathbf{C}_e$ is of full column rank. This condition warranties a successful elimination of contributions of $\mathbf{C}_e$, as we are going to show in the next subsection.

2.1 Convolution Kernel Compensation

Recall Eq. (2). It has a typical MIMO structure. From this point of view, $\mathbf{C}_e$ is a convolution kernel convolving $\mathbf{t}_e(n)$ to observations $\mathbf{y}_e(n)$. Given $\mathbf{y}_e$, if we can get rid of $\mathbf{C}_e$ the triggering instants of unknown source symbols, $\mathbf{t}_e$, would result. We called this process "convolution kernel compensation (CKC)".

Observe the following expression:

$$\mathbf{y}_e^T(n)\mathbf{R}_{\mathbf{y}_e}^{-1}\mathbf{y}_e(n) \tag{7}$$

where $\mathbf{R}_{\mathbf{y}_e}$ stands for the sample correlation matrix:

$$\mathbf{R}_{\mathbf{y}_e} = \mathbf{y}_e\mathbf{y}_e^T = \mathbf{C}_e\mathbf{t}_e\mathbf{t}_e^T\mathbf{C}_e^T + \sigma^2\mathbf{I} = \mathbf{C}_e\mathbf{R}_{\mathbf{t}_e}\mathbf{C}_e^T + \sigma^2\mathbf{I} \tag{8}$$

with $\mathbf{R}_{\mathbf{t}_e}$ denoting sample correlation matrix of source triggering trains of pulses, and the expression $\sigma^2\mathbf{I}$ stands for the correlation matrix of noise $\mathbf{v}_e$.

For easier comprehension of derivation, continue with the noise-free case. By substituting (8) into (7), we see that convolution kernel is eliminated:

$$\mathbf{y}_e^T(n)\mathbf{R}_{\mathbf{y}_e}^{-1}\mathbf{y}_e(n) = \mathbf{t}_e^T(n)\mathbf{C}_e^T\mathbf{C}_e^{-T}\mathbf{R}_{\mathbf{t}_e}^{-1}\mathbf{C}_e^{-1}\mathbf{C}_e\mathbf{t}_e(n) =$$

$$\mathbf{t}_e^T(n)\mathbf{R}_{\mathbf{t}_e}^{-1}\mathbf{t}_e(n) \tag{9}$$

The expression from (7) is known as Mahalanobius distance, which, as it is clear from Eq. (9), yields only the information on source triggering instants. Actually, its value depends on the number of sources active in given time instant n. This is why we call it *activity index*.

Suppose we deal with orthogonal sources and n_0 indicates the time instant where one of them generates a symbol (its contribution appears in the observation). Then vector $\mathbf{t}_e(n_0)$ is all zero except the element which belongs to the generated symbol, say the i-th, and equals 1. Besides, matrix $\mathbf{R}_{\mathbf{t}_e}$ is diagonal, and so is $\mathbf{R}_{\mathbf{t}_e}^{-1}$. It is then straightforward that

$$p_{n_0,i}(n) = \mathbf{y}_e^T(n_0)\mathbf{R}_{\mathbf{y}_e}^{-1}\mathbf{y}_e(n) = \mathbf{t}_e^T(n_0)\mathbf{R}_{\mathbf{t}_e}^{-1}\mathbf{t}_e(n) =$$

$$r_{i,i}t_{e,i}(n_0)t_{e,i}(n) = r_{i,i}t_{e,i}(n) \tag{10}$$

where $r_{i,I}$ denotes the i-th diagonal element of $\mathbf{R}_{\mathbf{t}_e}^{-1}$, and $t_{e,i}(n)$ stands for the train value at lag n for the i-th source symbol. Evidently, in Eq. (10) we have obtained a sequence $\mathbf{p}_{n_0,i}$ whose values equal the i-th source-symbol triggering pulse train to a constant amplitude factor, $r_{i,i}$. So, all repetitions of that symbol are detected.

The values of activity index indicate those lags n_i where individual sources contribute their symbols. If we select such n_i's that cover all different source contributions, a thorough decomposition is done and all source-symbol triggering pulse trains, $\mathbf{t}_i$; $i \in [1,K]$, are separated.

Let's also briefly discuss nonideal conditions. In ideal condition with orthogonal source-symbol contributions, no noise and the number of observations exceeding the number of different source-symbol contributions, the convolution kernel $\mathbf{C}_e$ is completely eliminated. If any of the ideal conditions cannot be met, $\mathbf{C}_e$ is not eliminated but only compensated to a certain extent. Consequently, the resulting decomposition of source-symbol triggering instants, Eq. (10), move off the ideal binary valued pulse train (sample values either 0 or $r_{i,i}$). Hence, the ideal Bernoulli distribution of any $\mathbf{p}_{n_i,j}$ tends to "smear", so the probability distribution of "no trigger" values may start overlapping the distribution of "trigger" values. A more detailed explanation goes beyond the scope of this paper, so we only stress here that even in far nonideal cases, such as with the signal-to-noise ratio as low as 0 dB, confidence level for the detection of source-symbol triggering instants remain above 98 %. Some additional results are given in the experimental part, Sections 3 and 4.

2.2 Extension to 2D Cases

As we have pointed out, analogy between source contributions in 1D and 2D observations can be found. 2D observations, i.e. images, can be interpreted as a compositum of several subimages appearing at different image co-ordinates. Thus, an image may be seen as a convolution of different regions and the corresponding "triggering" unit-samples whose positions in 2D determine the region placements within the image frame.

The most obvious way to implement CKC also in 2D is vectorization of images. Assume we have set of images $\mathbf{I}_k$; $k \in [1,M]$, and that $I_k(i,j)$ denotes the value of the k-th image pixel at (i,j) co-ordinates. Then

$$\mathbf{y}_k = vec(\mathbf{I}_k) \tag{11}$$

is a vector whose elements correspond to the concatenated rows of image $\mathbf{I}_k$, so that

$$vec(\mathbf{I}_k) = [I_k(0,0), I_k(0,1),\ldots,I_k(0,N_2-1),\mathbf{0},$$

$$I_k(1,0), I_k(1,1),\ldots,I_k(1,N_2-1),\mathbf{0},\ldots,$$

$$I_k(N_1-1,0), I_k(N_1-1,1),\ldots,$$

$$I_k(N_1-1,N_2-1)] \tag{12}$$

where N_1 and N_2 stand for image dimensions. Every row of pixels is padded by M_e zeros (denoted by vector **0**), where M_e means the extension factor from inequality (6).

The extension of vector $\mathbf{y}_k$ from Eq. (11) is performed the same way as for 1D case in Eq. (5). Also the other decomposition steps explained in Eqs. (7) to (10) can be implemented without modifications. A selected n_0 now determines location of a certain subimage region, with its 2D co-ordinates being transformed into n_0 by vectorization. The resulting sequence $\mathbf{p}_{n_0,i}$ comprises pulses at the positions indicating the repetitions of the subimage from location n_0. For optimal decomposition results, the number of observations, M, meaning different images of the same scene here, must exceed the number of different subimages.

It has to be emphasized that in Eq. (12) proposed image vectorization leads to a one-row vector, which limits the decomposition to subimages of one-row width only. At the same time, these subimages can extend at most across M_e image columns, because the CKC extension introduced in Eq. (5) "joins" the information of M_e subsequent samples. If the subimage regions of interest span larger areas, images have to be vectorized differently. They have to be segmented in such a way that the number of rows in every segment corresponds to the vertical dimension of the regions looked for. Every segment row is then taken as a separate observation entering the CKC-based decomposition. Consequently, only a single image segment is decomposed at a time, with no correlation to other segments. However, it is also possible for several image segments to be included into the same decomposition run. In this case, those segments have to be padded by M_e zeros and concatenated.

3 APPLICATION OF CKC TO THE SURFACE ELECTROMIOGRAM DECOMPOSITION

Human body contains different kinds of electrically excitable tissues, such as nerves and muscle fibres, which, when active, conduct measurable biopotentials, typically of length of several *ms*. These biopotentials can be detected either by inserting invasive needle electrodes into the tissue or by placing pick-up electrodes on the skin surface, above the investigated organ. Although being more selective, the invasive needle electrodes impose several restrictions to everyday clinical investigations. Firstly, measurements must be taken in a sterile environment and under supervision of trained physicians. Secondly, in order to reduce the tissue damage, there is a constant need for miniaturization of needle electrodes. This significantly increases the costs of manufacturing. Finally, the invasive recoding techniques put a lot of stress on an investigated subject and increase the fear from preventive clinical investigations (Merletti, 1994).

The aforementioned problems can be avoided by using less selective surface electrodes, providing signal processing techniques exists, which are capable of extracting clinically relevant information out of recorded data. Unfortunately, this is not a trivial task. Namely, the supportive tissues separating the investigated biological sources from the pick-up electrodes acts as a low pass filter and hinder the information in the detected signals. In addition, acquiring surface signals, contributions of different biological sources are detected. When electrical activity of skeletal muscles is observed, for example, we deal with several tens of sources (so called motor units, MU), simultaneously contributing their biopotentials (so called action potentials, AP) to the detected EMG interference pattern (Merletti, 1994). The decomposition of the surface EMG into the contributions of different MUs is, hence, a highly complex problem whose solution has been addressed with a many different methods. Unfortunately, most methods suffer from a drop of performance in case of significant superposition of MU action potentials.

Surface EMG signals can always be modeled by Eq. (1), provided they have been acquired during an isometric muscle contraction (De Luca, 1996). In such a model, observations $y_i(n)$ correspond to measured surface signals, $c_{ij}(n)$ corresponds to the action potential of the j-th MU, as detected by the i-th pick-up electrode, while $t_j(n)$ stands for a pulse sequence carrying the information about triggering times of APs. The length of detected APs, L, depends on the sampling frequency, but typically ranges from 15 to 25 samples when the Nyquist frequency is made equal to the bandwidth of the surface signals. At low contraction levels, different MUs discharge in relatively regular but random time instants, independently of each other. At higher contraction levels, the MUs start exhibiting weak tendency to synchronize, but this synchronization hardly exceeds the 5 % of its maximal possible value. As a result, $t_j(n)$ can be modelled as close-to-orthogonal random pulse sequences and the theory of 1D CKC method can be readily applied to the SEMG signals. This is further demonstrated by the

experimental results described in the next subsection.

3.1 Experimental Protocol

Nine healthy male subjects (age 26.8 ± 2.2 years, height 179 ± 7 *cm*, weight of 72.1 ± 8.3 *kg*) participated to our experiment. Surface EMG signals were acquired during isometric, constant-force contractions of the dominant biceps brachii muscle. In order to provide sufficient number of measurements, *M*, a matrix of 55 pick-up electrodes arranged in five columns and 11 lines (without the four corner electrodes) was used while all the contractions were performed at 5% and 10% of the maximum voluntary contraction (MVC) force. The EMG signals were recorded in longitudinal single differential configuration, amplified (gain set to 5000), band-pass filtered (3 *dB* bandwidth, 10 –500 *Hz*), and sampled at 2500 *Hz* by a 12 bit A/D converter. During signal acquisition, the noise and movement artefacts were visually controlled and reduced by applying water to the skin surface. Before any further processing, all the measurements were digitally filtered to suppress the power-line interference. Recorded signals are exemplified in Fig. 1.
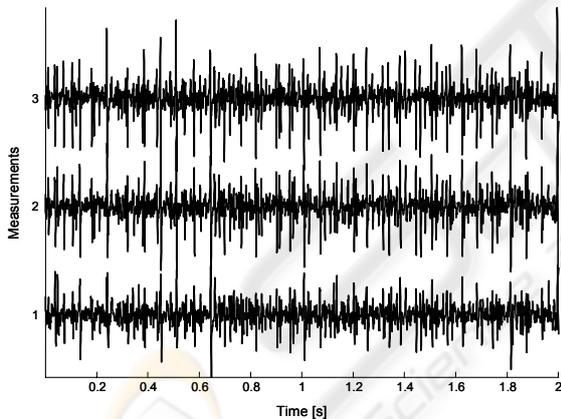
Figure 1: Real surface EMG signals recorded during isometric, low-level (10% MVC) contraction of dominant biceps brachii muscle.

The measured signals were extended according to Eq. (5) with extension factor, M_e, set to 10. In order to reconstruct the MU triggering pulses (Fig. 2), 1D CKC decomposition method was applied to the measured signals. The identified triggering pulses were then used by spike triggering sliding window averaging technique (Disselhorst-Klug, 1999) to reconstruct the MU APs as detected by different pick-up electrodes (Fig. 3 depicts the first decomposed AP as it contributes to each of 51 electrodes). Finally,

convolving the estimated AP shapes with the identified sequence of MU triggering pulses, the MU AP trains were reconstructed and compared to the original measurements (Figs. 4.a and 4.b). Rows 1 to 10 in Fig. 4 correspond to the ten decomposed MU APs depicted in the time instants when they trigger and contribute to the measured SEMGs. They are summed up in row 4.b).
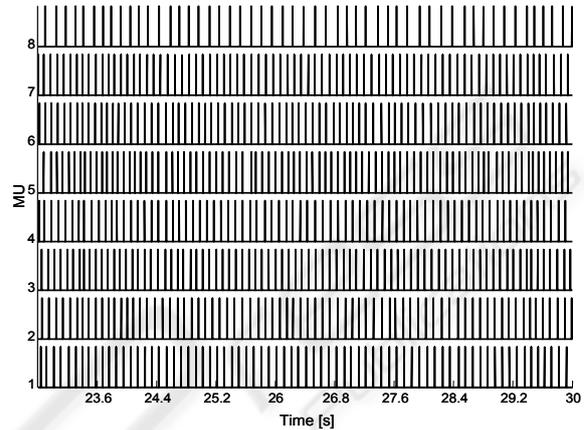
Figure 2: A part of MU triggering pulses (i.e. time instants in which the contributions of different MUs appeared in observations) reconstructed by the 1D CKC method from 30 s long real SEMG signals of dominant biceps brachii muscle (subject 3, 10% MVC measurement).
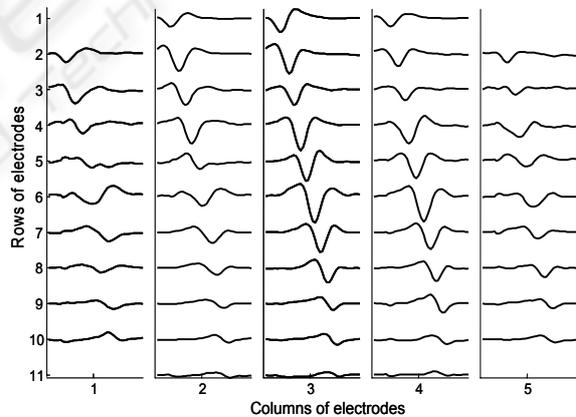
Figure 3: APs of MU 1 reconstructed by the spike triggered sliding window averaging technique (293 averages according to the train depicted in Fig. 2, bottom) from given 30 s long SEMG observations.

On average, 3.4 ± 1.3 (mean $\pm$ standard deviation) and 6.2 ± 2.2 MUs were identified during the contractions at 5% and 10% MVC, respectively. The exact number of active MUs is, of course, unknown. Nevertheless, comparing the energies of the identified MU action potentials with the energy of the original signal we can approximately estimate the percentage of the information that was extracted from the surface EMG

signals. The average ratio yielded $71 \pm 15\%$, proving that the largest SEMG components were identified (Fig. 4). Most of the identified MUs showed decreasing firing frequency over time (presumably due to fatigue).
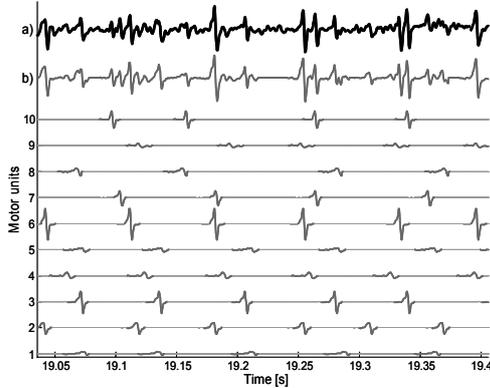
Figure 4: Contributions of different MUs identified by the 1D CKC method from 30 s long real SEMG signals recorded during isometric, 10% MVC measurement of the dominant biceps brachii (subject 8); a) the originally observed SEMG signal, b) sum of the identified MU contributions.

Finally, the shapes of the MU action potentials as detected by the different electrodes were stable over time and indicated anatomical and physiological MU properties, such as location of innervation zones, length of the fibres, and muscle fibre conduction velocity (Fig. 3).

4 APPLICATION OF CKC TO RANGE IMAGING

Human beings depend on stereo vision for observing their surroundings. Slight displacement of images enables them to reliably detect range information, which can be used to their advantage. In computer vision, the same effect is used to reconstruct the range or depth image of a scene based on two or more input images. Range reconstruction can be formulated as a matching problem between pixels of the left and right stereo image. In general, the problem doesn't have a unique solution due to lack of image texture, occlusions, periodic image structures and noise (Šara, 2002). Early algorithms avoided those problems by reconstructing only sparse range images (Sonka, 1994). Modern applications, such as image-based modelling, texture mapping of 3D objects and similar, require dense range images, where disparity of almost all image pixels is known. To alleviate this problem, several constraints are commonly used. All the surfaces in the scene are supposed to be Lambertian, the geometry of the stereosystem should be known (calibrated camera) and range values are expected to change smoothly, without sharp jumps (Gutierrez, 2003).

Using the geometric properties of the stereosystem, it can be shown that the matching space can be reduced to two epipolar image rows (Jain, 1995). Each image row can easily be represented as an observation $\mathbf{y}_k$, extended and decomposed by the CKC method, referring to the extension introduced in Subsection 2.2. In order to detect disparity of every pixel, its position in the left image row is described by index n_0 and the pulse train $\mathbf{p}_{n_0,i}$ is calculated according to Eq. (10) along the right epipolar image row. Ideally, the sequence $\mathbf{p}_{n_0,i}$ contains only one sharp impulse. This pulse indicate the most probable location n_1 of the subimage which best corresponds in the right stereo image to that selected by index n_0 in the left image (Fig. 5). Disparity of pixel n_0 is, therefore, calculated as

$$Disp(n_0) = n_0 - n_1. \qquad (13)$$

In order to achieve more reliable and robust results, the matching is repeated using the right stereo image as a starting point. Only pixels with consistent left-to-right and right-to-left matches are assigned the final disparity value.
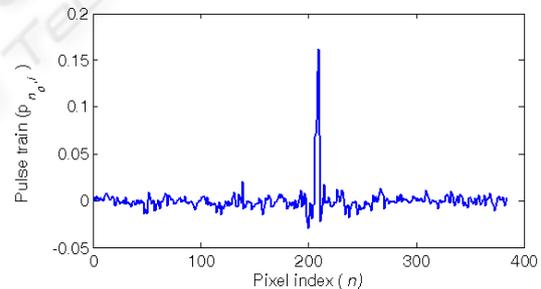
Figure 5: An example of a pulse train $\mathbf{p}_{n_0,i}$, as obtained for a selected row in the right image. The location of the pulse determines the location of a suitable subimage region.

As we have explained in Subsection 2.2, the shape of image regions being matched by our CKC approach is determined by the number of image rows included in one decomposition run, and by the extension factor M_e. The quality of left-right stereo-image matching depends on the appearance of the same image regions in both left and right images. This appearance may not be equally good for smaller or larger sections of an image object. So, it can be expected that its depth may be misinterpreted owing to inferior quality of matching. However, if we observe a part of

an object in different sizes, so with different size of regions inserted in the CKC-based matching, the information of best fit can be compared for different region sizes. Thus, the most probable disparity can be estimated, which is the idea followed by our 2D CKC range imaging, as exemplified in the next subsection.

4.1 Experiments with CKC-based range imaging

All experiments were performed on the test images from the Middlebury Stereo Vision Page (Scharstein, 2002). This test set provides reliable reference data and is very popular in the research community, enabling the comparison of different range reconstruction techniques. The results of our CKC-based approach are depicted in Fig. 6.

a)

b)
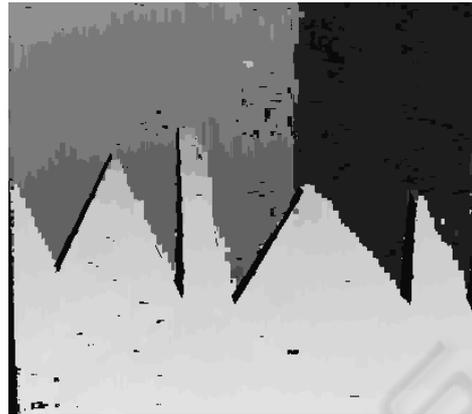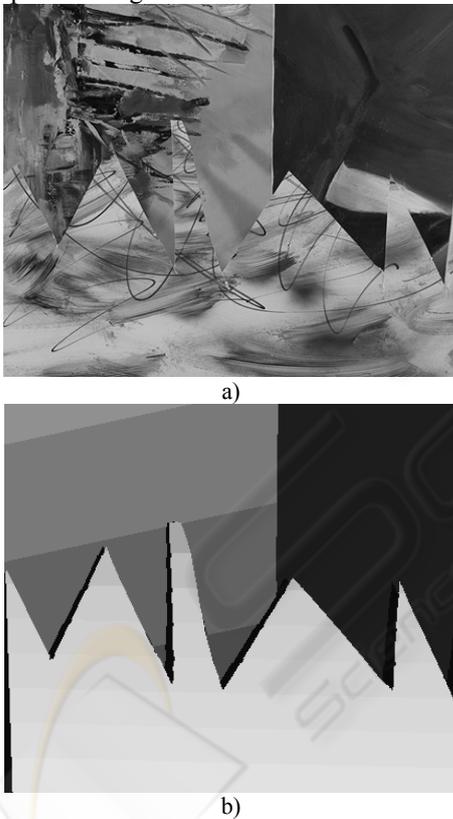
c)

Figure 6: An example of reconstructed range image on the SAWTOOTH stereo test set: (a) left input image, (b) reference range image, and (c) the resulting CKC-based range image.

In Table 1, they are compared to results of the standard correlation-based approach using the following performance metrics:

o percentage of image pixels with consistent left-to-right and right-to-left matches,
o percentage of matched pixels whose disparity differs from the reference value by more than 1 pixel,
o RMS of disparity difference between matched pixels and the reference image.

Table 1: Comparison of disparity values, obtained the 2D CKC method and a typical correlation-based approach (SSD, 5×5 window). Mean values for four test images (MAP, TSUKUBA, VENUS, SAWTOOTH) are shown.

Algorithm	Matches found (%)	Bad matches (%)	RMS disparity difference (pixels)
CKC	91.3 ± 12.1	1.6 ± 0.4	3.4 ± 2.5
SSD	78.2 ± 14.2	2.0 ± 0.5	7.9 ± 4.5

5 CONCLUSIONS

We derived a novel method for statistical signal processing which blindly separates source contributions superimposed in one or more available observations. It is based on the correlation of

observations, so that the inverse of correlation matrix is used to compensate the convolution kernel influence. The method tolerates moderate declines of sources from the orthogonality, and copes with considerable amount of additive random noise.

1D version of our CKC approach was applied to the decomposition of real surface EMG signals. The reported results demonstrate the CKC method is not sensitive to superimpositions of MU action potentials and has high potential in clinical applications for the non-invasive analysis of single MU properties.

In this paper we also derived a 2D version of CKC. It makes use of all the benefits mentioned above also for image processing. One of possible applications is searching equivalent regions in more images, whereas the matching on a pair of stereo images directly imposes a new range imaging technique. We exemplified it by constructing range images for a set of reference images. The obtained results are comparable with other known approaches, but because of the CKC being rather noise resistant, the new way of range imaging obtains a better robustness.

Recent investigations prove that the CKC performance can be improved by combining it with non-linear modifications of observations and by non-linear modelling instead of present MIMO scheme. Our research continues in this direction.

REFERENCES

Madhow, U., 1998. Blind Adaptive interference suppression for direct-sequence CDMA. In *Proceedings of the IEEE*, 86 (10), 2049-2069.

Desodt G.., Muller D., 1994. Complex independent components analysis applied to the separation of radar signals. In *Signal Processing V, Theories and applications*, 665-668.

Gribonval R., 2002. Sparse decomposition of stereo signals with matching pursuit and application to blind separation of more than two sources from a stereo mixture. In *Proceedings of ICASSP'02*.

Barros A. K., Mansour A., Ohnishi N., 1999. Removing artefacts from ECG signals using independent components analysis. In *Neurocomputing*, 22, 173-186.

Hyvärinen A., Inki M., 2002. Estimating overcomplete independent component bases for image windows. In *Journal of Mathematical Imaging and Vision*, 17, 139-152.

Cardoso J. F., 1998. Blind signal separation: statistical principles. In *Proceeding of the IEEE, Special issue on blind identification and estimation*, 9 (10), 2009-2025.

Belouchrani A., Meraim K. A., Cardoso J. F., Moulines E., 1997. A blind source separation technique based on second order statistics. In *IEEE Transactions on signal processing*, 45 (2), 434-444.

Holobar A., Zazula D., 2004. Correlation-based approach to separation of surface electromyograms at low contraction forces. In *Med. & Biol. Eng. & Comput.*, 42 (4), 487-496.

Merletti R., 1994. Surface electromyography: possibilities and limitations. In *J. of Rehab. Sci.*, 7 (3), 25-34.

De Luca C. J., Foley P. J., Erim Z., 1996. Motor unit control properties in constant-force isometric contrac-tions. In *J. of Neurophysiol.*, 76 (3), 1503-1516.

Disselhorst-Klug C., Rau G.., Schmeer A., Silny J., 1999. Non-invasive detection of the single motor unit action potential by averaging the spatial potential distribution triggered on a spatially filtered motor unit action potential. In *J. of Electromyogr. and Kinesiol*, 9, 67-72.

Kay S. M., 1993. *Fundamentals of Statistical Signal Processing*, Prentice-Hall International. London.

Šara R., 2002. Finding the largest Unambiguous Component of Stereo Matching. In *European Conference on Computer Vision*, LNCS 2352, 900-914.

Sonka M., Hlavac V., Boyle R., 1994. *Image Processing, Analysis and Machine Vision*, Chapman & Hall. London.

Gutierrez S., Marroquin J. M., 2003. Disparity estimation and reconstruction in stereo vision. In *Technical report*, Centro de Investigacion en Matematicas, Mexico.

Jain R., Kasturi R., Schunck B. G., 1995. *Machine Vision*, McGraw-Hill Inc. International Edition.

Scharstein D., Szeliski R., 2002. A Taxonomy and Evaluation of Dense Two-Frame Stereo Correspondence Algorithms. In *International Journal of Computer Vision*, 47, 7-42.